Design Aspects of Bearingless Torque Motors

Siegfried Silber*, Wolfgang Amrhein
Institute of Electrical Drives and Power Electronics
Johannes Kepler University Linz
Shareholder of the ACCM GmbH
Linz, Austria

Herbert Grabner, Robert Lohninger
Linz Center of Mechatronics
Shareholder of the ACCM GmbH
Linz, Austria

Abstract

In this paper novel topologies of multiphase bearingless motors featuring outstanding motor efficiency and high radial force capacity are presented. For a systematic layout a simple design guideline is provided. These motors are especially suitable for applications where high torque at relatively low speed is demanded, therefore this configuration is referred to as bearingless torque motor. Since there are no dedicated bearing and motor windings the winding scheme becomes very simple and is furthermore characterized by concentrated coils only.

Motor designs with different pole and slot configurations are compared by means of appropriate performance indexes. For the most promising design a demonstrator was manufactured and tested.

1 Introduction

The reliability of electrical drives has been improved significantly with gearless direct drives during the last few years. Especially direct inverter-fed drives gained popularity because of reduced maintenance costs and higher lifetime since a gearbox can be omitted. These drives are typically equipped with motors featuring high torque per volume – so-called torque motors. High torque capacity can be achieved with special motor topologies and certain slot and pole configurations as for instance described in [1, 2, 3]. A further step improving reliability is the elimination of mechanical bearings, which could offer significant advantages for certain applications. Amongst these are handling systems used in vacuum, mixers for the chemical and pharmaceutical industries as well as pumps and blowers. The most compact and thus cost-effective solution of such a drive can be achieved by employing a bearingless motor where some degrees of freedom (DOF) are stabilized passively. Normally, the radial DOFs of such bearingless motors are stabilized actively and the axial and tilting DOFs are stabilized passively due to the reluctance forces of permanent magnets [4]. During the last 20 years several different motor design based on that principle have been developed [5, 6, 7, 8, 9]. However, these designs either have a complicated winding configuration with separate motor and bearing windings or have low torque capacity. Only recently new bearingless motor designs have appeared that are suitable for applications where high torque at low speed is demanded [10, 11, 12]. In this paper a novel topology of a bearingless motor that features even better efficiency and higher radial forces compared to existing designs is presented.

2 Motor Design

Conventional motors, supported by ball bearings, with a high number of poles operated at relatively low speeds are often referred to as torque motors. A wide variety of different distributed and concentrated winding configurations has been implemented for these motors. For

*Contact Author Information: siegfried.silber@jku.at, Johannes Kepler University of Linz, Altenbergerstrasse 69, 4040 Linz, Austria, phone: +43 732 2468 6429

N_s	$2p$	ξ^1	Radial force
15	14	0.951	yes
15	16	0.951	yes
18	16	0.945	no
18	20	0.945	no
21	20	0.953	yes
21	22	0.953	yes
24	22	0.949	no
24	26	0.949	no

Table 1: Fundamental winding factor ξ^1 for three phase motors with N_s stator slots and $2p$ poles.

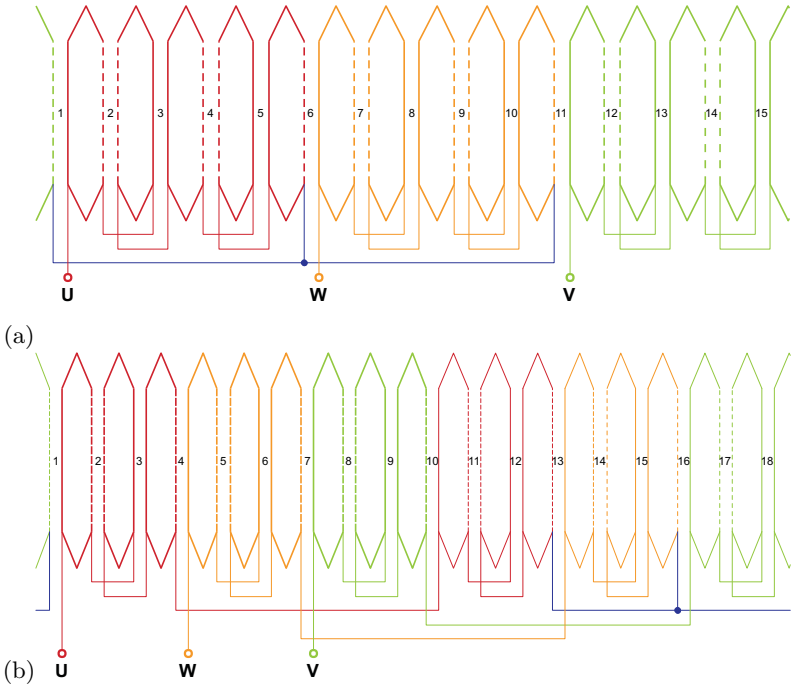

Figure 1: Winding schemes for conventional three phase motors. (a) 15 slots and 16 poles. (b) 18 slots and 16 poles.

particular pole slot combinations the fundamental winding factor almost becomes one even for concentrated windings which have a significant advantage over distributed ones because of the reduced winding head, thus leading to better efficiency.

Some typical slot pole combinations are given in Table 1, where N_s denotes the number of slots and $2p$ is the number of poles. The fundamental winding factor ξ^1 is also stated in Table 1 and from the last column it can be seen if the motor topology generates radial forces during normal operation. Two windings schemes, for 15 and 18 slots and 16 poles each, are depicted in Fig. 1. The significant difference between these two winding configurations is that the one with 15 slots generates radial forces. Normally, unsymmetrical winding configurations

that produce radial forces are not used for conventional motors because of undesired acoustic noise. Especially, when each phase covers a sector of 120 degrees (for a three phase motor), as it does in the present configuration, the undesired radial forces become quite high. This undesired side-effect, however, can be utilized to actively generate radial forces for the levitation of the rotor. But it is obvious that with only three phases independent generation of torque and radial forces in two directions is not feasible, because for a star-connected winding only two currents are independent. Thus, for a bearingless operation at least four motor phases are required.

The proposed bearingless torque motor is characterized by a multi-phase winding system with concentrated coils where each phase is wound in

$$\frac{N_s}{m} \tag{1}$$

adjacent slots only. Moreover, each phase covers a sector of

$$\frac{360}{m} \tag{2}$$

angular degrees, where m denotes the number of motor phases. For a systematic motor design a simple guideline can be provided: Generally, the number of slots must be a multiple of the number of phases. Then the number of pole pairs p should meet the condition

$$p = \frac{N_s}{2} \pm 1 \qquad \text{if } N_s = 2k,\ \forall k \in \mathbb{N}, \tag{3}$$

for an even number of slots and

$$p = \frac{N_s \pm 1}{2} \qquad \text{if } N_s = 2k+1,\ \forall k \in \mathbb{N} \tag{4}$$

for an odd number of slots. Finally the coils of each phase are located in adjacent slots only, even if this leads to a lower fundamental winding factor. For a winding system with 24 slots, 13 pole pairs and 6 phases the optimal configuration concerning the winding factor is shown in Fig. 2 (a) and the winding configuration according to the proposed design guideline is illustrated in Fig. 2 (b). The difference in the fundamental winding factor is $\xi^1 = 0.983$ for the optimal winding scheme and $\xi^1 = 0.949$ for a bearingless torque motor configuration. The latter is equivalent to a conventional motor with three phases.

Simplified Analytical Force and Torque Model

For a design study, normally, many different configurations of bearingless motors have to be evaluated. A methodical evaluation approach should preferably be based on suitable performance indexes and an estimate of the production costs. An additional requirement of the evaluation process is that it should be simple and should not consume too much CPU time. For this reason complex calculation methods like 3D FEM analysis are not useful for deriving the performance indexes required. In contrast to published accurate analytical force and torque models for bearingless motors [13, 14] in this paper a simplified analytical model based on 2D FEM calculations is proposed.

For a bearingless motor with surface-mounted permanent magnets where the stator iron is not driven into saturation a linear relationship between phase currents and radial forces and torque can be found. For this purpose the forces and torque acting on the rotor are calculated by

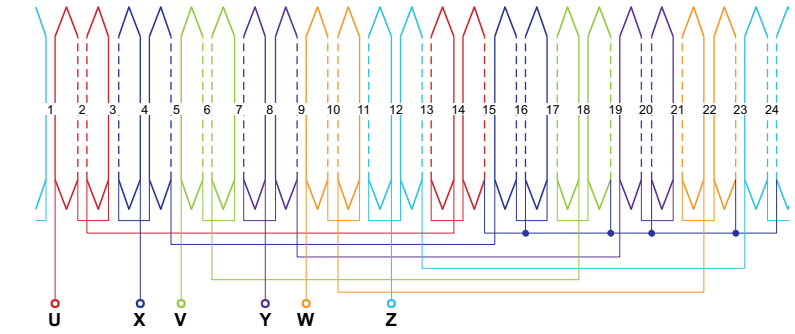

(a)

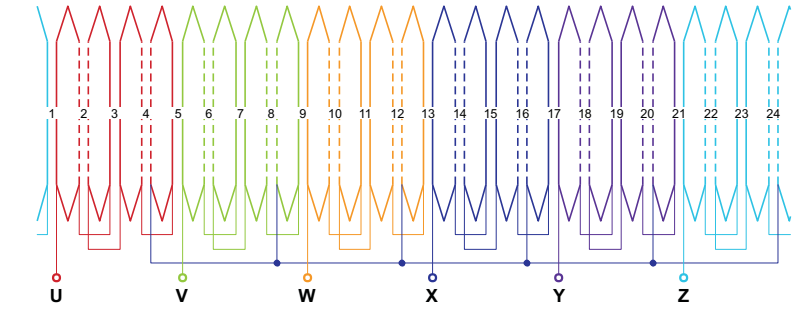

(b)

Figure 2: Winding schemes for 24 slots, 26 poles and 6 phases. (a) Configuration for the highest fundamental winding factor $\xi^1 = 0.983$. (b) Configuration according to the proposed design guideline $\xi^1 = 0.949$.

2D FEM when only one phase is fed with constant current. A relationship between a constant current through phase one and the resulting forces and torque can be expressed as

$$\mathbf{T}_{m,1}(\theta_r) = \frac{1}{I_{11}} \begin{bmatrix} F_{rx}(\theta_r,\, I_{11}) \\ F_{ry}(\theta_r,\, I_{11}) \\ T_r(\theta_r,\, I_{11}) \end{bmatrix} \tag{5}$$

where $F_{rx}(\theta_r,\, I_{11})$, $F_{ry}(\theta_r,\, I_{11})$ and $T_r(\theta_r,\, I_{11})$ denote the forces acting on the rotor in radial directions and the torque for a constant current I_{11} through phase one, respectively. $\mathbf{T}_{m,1}(\theta_r)$ represents the relationship between forces and torque (generalized forces) and the current written in vector notation as a function of the electrical rotor angle θ_r. This relationship is simplified so that it is only a function of the rotor angle. For this simplified model the rotor has to be in the magnetic center of the stator. Furthermore, cogging torque is neglected.

This linear approximation has sufficient accuracy for motors with a large air gap and surface-mounted permanent magnets. The reason is that the flux density caused by the coils is small compared with the flux density of the permanent magnets. When the calculation of the forces and torque is done consecutively for all m phases a simple current to force and torque relationship can be found by combining the generalized force functions into a matrix of the form

$$\begin{bmatrix} F_{rx}(\theta_r) \\ F_{ry}(\theta_r) \\ T_r(\theta_r) \end{bmatrix} = \begin{bmatrix} \mathbf{T}_{m,1}(\theta_r) & \mathbf{T}_{m,2}(\theta_r) & \dots & \mathbf{T}_{m,m}(\theta_r) \end{bmatrix} \mathbf{i}_1 \tag{6}$$

with the vector

$$\mathbf{i}_1 = \begin{bmatrix} i_1 & i_2 & \cdots & i_m \end{bmatrix}^{\mathrm{T}} \tag{7}$$

of the instantaneous phase current values. Further simplification can be achieved by a matrix notation

$$\mathbf{Q} = \mathbf{T}_m \mathbf{i}_1 \tag{8}$$

with

$$\mathbf{Q} = \begin{bmatrix} F_{rx}(\theta_r) \\ F_{ry}(\theta_r) \\ T_r(\theta_r) \end{bmatrix}, \qquad \mathbf{T}_m = \begin{bmatrix} \mathbf{T}_{m,1}(\theta_r) & \mathbf{T}_{m,2}(\theta_r) & \dots & \mathbf{T}_{m,m}(\theta_r) \end{bmatrix} \tag{9}$$

For the operation of a bearingless motor in a closed control loop it is necessary to supply the motor phases with such currents that generate desired radial forces and torque. In a mathematical sense this requires that equation (8) has to be solved for the phase currents $\mathbf{i}_1$. However, a unique solution of the form

$$\mathbf{i}_1 = \mathbf{T}_m^{-1} \mathbf{Q} \tag{10}$$

can only be found if the bearingless motor has three phases. Unfortunately, the bearingless motors that are under consideration in this paper have more than three phases. This means that any desired radial force and torque might be realized by many different sets of phase currents. Since many solutions might be possible it is the task to find a set of currents that generates the required radial forces and torque in the best way. One feasible solution to finding the best set of currents is to minimize the resistive power losses. This leads to the following optimization problem:

$$\min_{\mathbf{i}_1} \mathbf{i}_1^{\mathrm{T}} \mathbf{R}_1 \mathbf{i}_1 \tag{11}$$

subject to

$$\mathbf{T}_m \mathbf{i}_1 - \mathbf{Q} = \mathbf{0} \ , \tag{12}$$

where $\mathbf{R}_1$ is the matrix of the phase resistances. The solution to this optimization problem yields [15]

$$\mathbf{i}_1 = \mathbf{K}_m(\theta_r) \mathbf{Q} \ , \tag{13}$$

with the decoupling matrix

$$\mathbf{K}_m(\theta_r) = \mathbf{T}_m^{\mathrm{T}} \left(\mathbf{T}_m \mathbf{T}_m^{T} \right)^{-1} . \tag{14}$$

With the motor concepts that are considered in this paper star connection of the motor phases leads to a simplified inverter topology. For these types of bearingless motors the sum of the phase currents is restricted to zero for any mode of operation. To meet this additional requirement it is possible to impose an extra constraint on the optimization problem of the form

$$\begin{bmatrix} 1 & 1 & \cdots & 1 \end{bmatrix} \mathbf{i}_1 = \mathbf{1}^{\mathrm{T}} \mathbf{i}_1 = 0 \tag{15}$$

to force the sum of the phase currents to zero. Solving the optimization problem leads to the following decoupling matrix

$$\mathbf{K}_m(\theta_r) = \left(\mathbf{T}_m^{\mathrm{T}} - \frac{1}{m} \mathbf{1}\mathbf{1}^{\mathrm{T}} \mathbf{T}_m^{\mathrm{T}} \right) \left(\mathbf{T}_m \left(\mathbf{T}_m^{\mathrm{T}} - \frac{1}{m} \mathbf{1}\mathbf{1}^{\mathrm{T}} \mathbf{T}_m^{\mathrm{T}} \right) \right)^{-1} . \tag{16}$$

3 Performance Indexes

In many cases, the required torque and bearing forces can be generated by motor designs that differ in the winding configurations, the number of poles, and even in the number of phases. Furthermore, the motor design also has an impact on the inverter topology. For the evaluation of different motor designs performance figures or performance indexes have been introduced in [9]. For the current study, however, additional performance indexes are proposed for the comparison of the bearingless torque motors according to the guideline as described above.

To minimize the cost of the inverter it is important that for a given DC link voltage the RMS values of the phase currents are as low as possible. With regard to the motor this means that the torque and force constants are high. To account for asymmetric motor designs the force constant is calculated by an average of the RMS current to generate 1 N in the two radial directions

$$\mathbf{I}_1|_{F_{rx}=1\mathrm{N}} = \mathrm{rms}(\mathbf{K}_m \begin{bmatrix} 1 & 0 & 0 \end{bmatrix}^{\mathrm{T}}) \tag{17}$$

$$\mathbf{I}_1|_{F_{ry}=1\mathrm{N}} = \mathrm{rms}(\mathbf{K}_m \begin{bmatrix} 0 & 1 & 0 \end{bmatrix}^{\mathrm{T}}). \tag{18}$$

This results in a force constant of

$$k_F = \frac{2\,m}{\sum_{i=1}^{m}\sum_{j=1}^{2}\mathrm{rms}(\mathbf{K}_{m_{i,j}})}. \tag{19}$$

Consequently, the torque constant is calculated by

$$k_T = \frac{m}{\sum_{i=1}^{m}\mathrm{rms}(\mathbf{K}_{m_{i,3}})}. \tag{20}$$

For maximum temperature in the motor the losses at a specified operating point are of major interest. In this study, however, only the copper losses at nominal torque are considered. Details about the derivation of the copper losses for bearingless motors can be found in [9].

4 Comparison of Bearingless Torque Motor Configurations

In this section, different embodiments of bearingless torque motors are compared with regard to the performance indexes. The analysis, however, is limited to motors with 5 and 6 phases. To obtain comparable results some assumptions have to be made:

- Rotor diameters and the stator bores are the same for all motor designs.
- The volume of the magnetic material is the same.
- The load point characterized by speed and torque is equal.
- The peak value of the flux density in the stator teeth is 1.5 T.
- The copper area is constant. However, the mass of copper is different because of the different dimensions of the stator teeth.

		Unit	**M1**	**M2**	**M3**	**M4**	**M5**	**M6**
Phases	m		6	6	6	6	5	5
Slots	N_s		12	12	24	24	25	25
Poles pairs	p		5	7	11	13	12	13
Winding factor	ξ^1		0.933	0.933	0.949	0.949	0.982	0.982
Force constant	k_F	N/A	1.0	20.1	0.4	19.9	0	15.3
Torque constant	k_T	Nm/A	1.41	1.37	1.44	1.36	1.08	1.04
Copper loss	P_{cu}	W	59	56	54	67	56	62
Mass copper	m_{cu}	g	660	640	465	455	455	450

Table 2: Comparison of different motor topologies.

- The DC link voltage is the same for all motors.

To simplify the power inverter the motor phases are preferably connected to star [16]. Better utilization of the DC link voltage can be obtained by shifting the potential of the star point. This is, however, only feasible for an odd number of motor phases [17] and results in an amplitude of the phase voltages

$$\hat{U}_{11} = \frac{U_{DC}}{2\sqrt{2}} \frac{1}{\cos(\frac{\pi}{2m})}, \qquad \text{if } m = 2k+1,\ \forall k \in \mathbb{N}, \tag{21}$$

for an even number of motor phases the amlitude is lower

$$\hat{U}_{11} = \frac{U_{DC}}{2\sqrt{2}}, \qquad \text{if } m = 2k,\ \forall k \in \mathbb{N}, \tag{22}$$

where U_{DC} denotes the DC link voltage. Because of the symmetry of the motors with 6 phases the windings may be split into two independent three-phase windings (with two independent star points), shown in Fig. 5. Thus the peak value of the phase voltage results in

$$\begin{aligned} \hat{U}_{11} &= 0.372\, U_{DC} \quad \text{for } m = 5 \\ \hat{U}_{11} &= 0.408\, U_{DC} \quad \text{for } m = 6. \end{aligned}$$

The evaluation of the performance indexes for six different motor topologies is summarized in Table 2. The different motor designs are denoted as M1 to M6. Though the winding factors of the topologies with 5 phases is higher, motor topology **M4**, featuring 24 slots and 13 pole pairs, performs best. Therefore, this motor design is used for all further investigations. There are also certain configurations where force generation is not feasible (M1, M3 and M5) because the matrix $\mathbf{T}_m$ is badly conditioned.

5 Integration of Position Sensors

For closed loop operation of the bearingless torque motor radial displacement sensors and a rotor angle sensor are required. Normally, these sensors have to be located somewhere outside the air gap axially displaced, leading to an increased axial length of the motor. For the proposed bearingless torque motor topology each phase is located in a sector of adjacent slots. Owing to this particular phase distribution the slot opening at the margin between two phases may be increased and this space can be used for position sensors. To find a suitable gap angle where

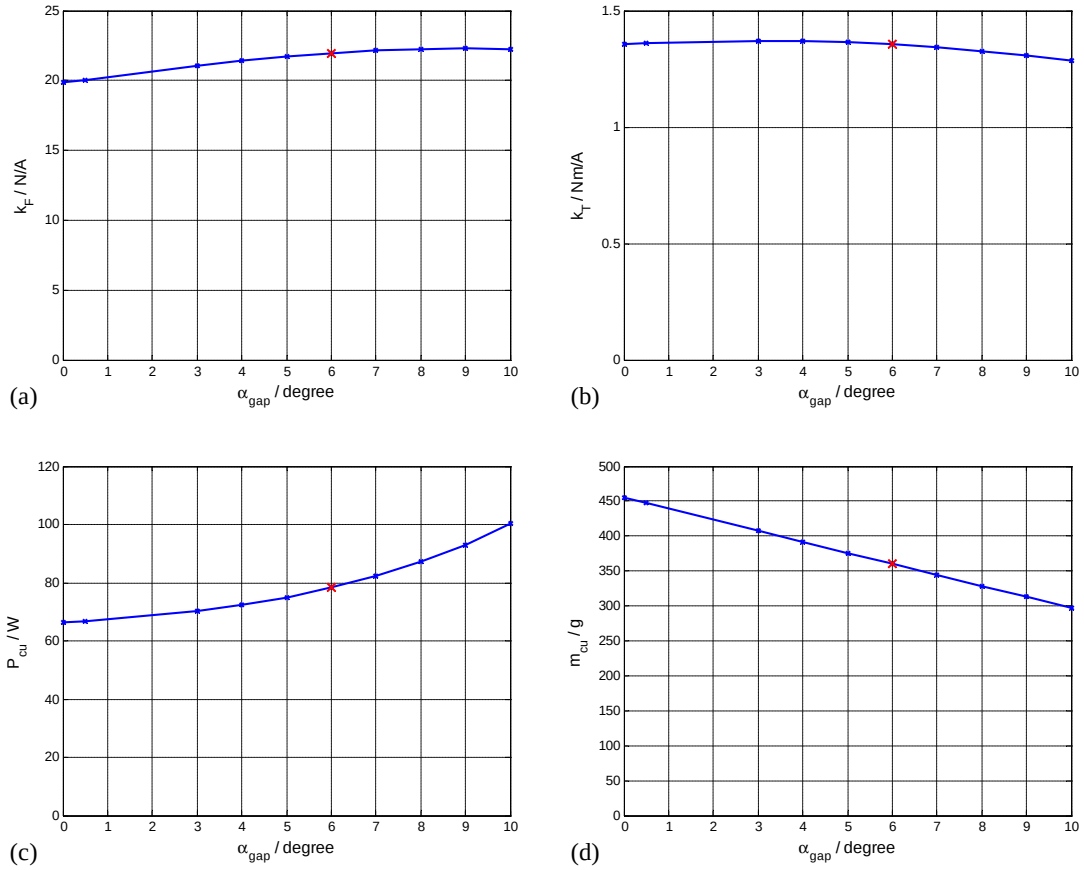

Figure 3: Performance indexes as a function of an increased slot opening α_{gap} at the margin between two phases for motor topology M4. (a) Force constant k_F. (b) Torque constant k_T. (c) Copper losses P_{cu}. (d) Mass of copper m_{cu}.

the performance indexes are still acceptable the performance indexes are plotted with respect to the gap angle α_{gap} in Fig. 3. These plots refer to motor topology **M4**. It is interesting that with an increased gap between the phases the force constant k_F gets even better, the torque constant k_T keeps almost constant, but the copper losses increase. The reason for the higher force constant is that force is generated in a smaller sector leading to a higher value of the projected force vectors. Copper losses are reduced because the copper area has to be reduced and hence the copper mass is reduced, too. As shown in Fig. 3 a gap angle of 6 degrees is a good compromise between space required for the position sensors and increase in copper losses (points marked in color red). The cross section of the selected bearingless torque motor and the corresponding winding scheme with two independent three-phase systems with separate star points are depicted in Fig. 4 and Fig. 5, respectively.

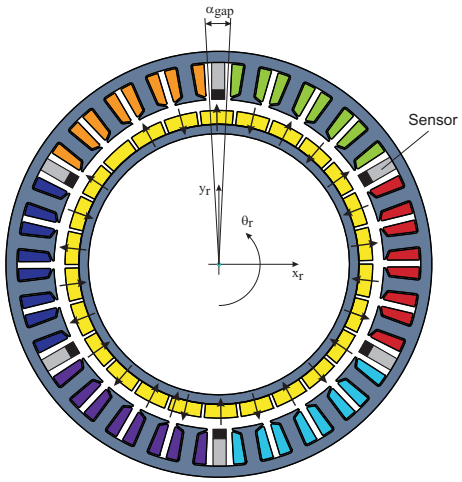

Figure 4: Cross section of the bearingless torque motor with a gap angle of 6 degrees.

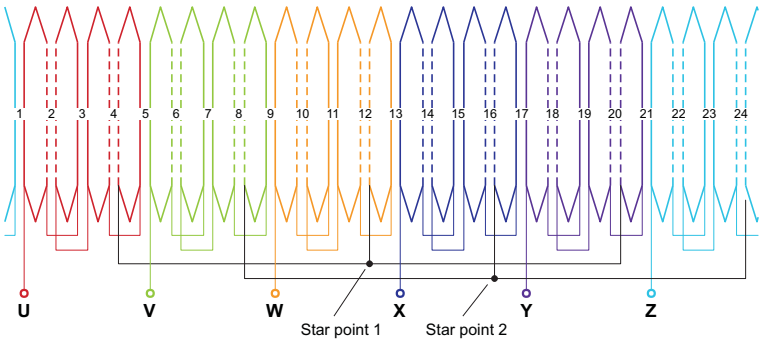

Figure 5: Winding scheme of the motor according to Fig. 4 with two independent three phase systems and separate star points.

6 Experimental Results

To verify the theoretical results a demonstrator of motor topology M4 with increased slot opening of 6 degrees was built. The motor with the detached rotor is shown in Fig. 6. The mechanical design of the electromagnetic parts is ready for industrial production. Moreover, the copper fill factor of the slots is low to be suitable for industrial needle winding technology. For comparison the forces at a constant current of 3 A through phase U was measured and the force terms (first two elements) of (5) were compared with results of a 2D FEM simulation, as depicted in Fig. 7. According to (19) and (20) the force and torque constants are caculated and summarized in Table 3. The simulation error is lower than 5 percent, furthermore the waveforms of the current to force relationship agree well.

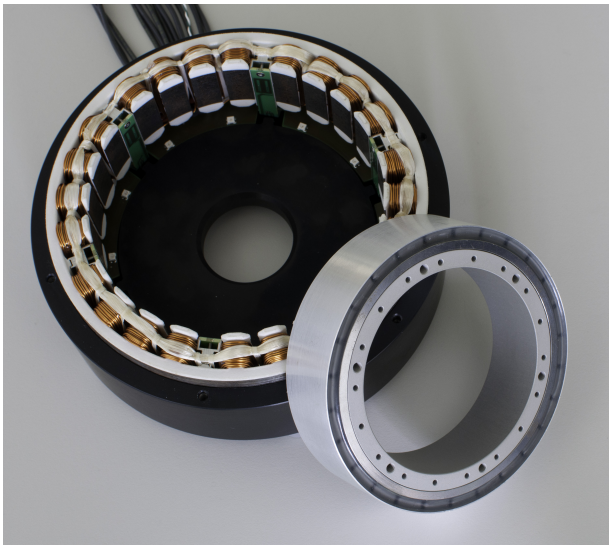

Figure 6: Prototype of motor topology M4 with an increased slot opening of 6 degrees.

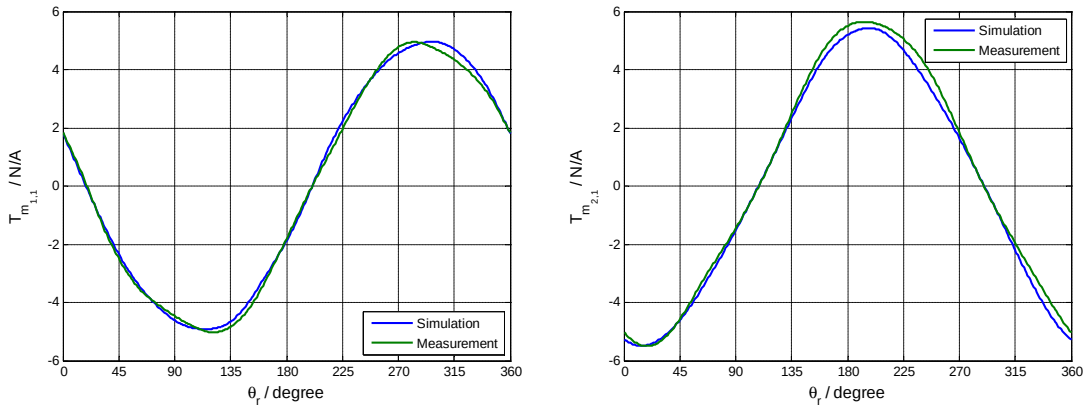

Figure 7: Simulated and measured current to force relationship.

		Unit	Simulation	Measurement	Error
Force constant	k_F	N/A	21.9	22.1	0.9%
Torque constant	k_T	Nm/A	1.35	1.29	4.7%

Table 3: Comparison of simulated and measured performance indexes.

7 Conclusion

By means of a simple design guideline derived in this paper, different motor topologies that are especially suitable for applications demanding high torque at relatively low speed are compared. In contrast to the majority of existing bearingless motor configurations these topologies do not have separate dedicated motor and bearing windings, but there are common windings where each phase consists of concentrated coils wound in adjacent slots only. Assessment of different motor topologies was done by appropriate performance indexes. The most promising motor design with 24 slots and 13 pole pairs was selected and analyzed in more detail. By means of a prototype the simulation results have been verified.

8 Acknowledgment

This work was mainly conducted within the research project "Nachhaltig ressourcenschonende elektrische Antriebe durch höchste Energie- und Material-Effizienz" (sustainable and resource-saving electrical drives through high energy and material efficiency) and is sponsored within the EU program "Regionale Wettbewerbsfähigkeit OÖ 2007-2013 (Regio 13)" by the European Regional Development Fund (ERDF) and the Province of Upper Austria. Parts of the work have been carried out within the Austrian Center of Competence in Mechatronics (ACCM), which is part of the COMET K2 program of the Austrian Government.

References

[1] J. Shi, F. Chai, X. Li, and S. Cheng. Study of the number of slots/pole combinations for low speed high torque permanent magnet synchronous motors. In *Electrical Machines and Systems (ICEMS), 2011 International Conference on*, pages 1 –3, Aug. 2011.

[2] J. Xia, T. Dong, C. Wang, and J. Zhao. Low speed high torque pmsm design based on unequal teeth structure. In *Electrical Machines and Systems, 2008. ICEMS 2008. International Conference on*, pages 3274 –3277, Oct. 2008.

[3] R. Wrobel and P.H. Mellor. Design considerations of a direct drive brushless machine with concentrated windings. *Energy Conversion, IEEE Transactions on*, 23(1):1 –8, March 2008.

[4] R. Schöb and N. Barletta. Principle and application of a bearingless slice motor. *JSME (The Japan Society of Mechanical Engineers) International Journal*, 40(4):593–598, 1997.

[5] M.T. Bartholet, T. Nussbaumer, S. Silber, and J.W. Kolar. Comparative evaluation of polyphase bearingless slice motors for fluid-handling applications. *Industry Applications, IEEE Transactions on*, 45(5):1821 –1830, Sept.-Oct. 2009.

[6] W. Gruber, W. Amrhein, and M. Haslmayr. Bearingless segment motor with five stator elements - design and optimization. *Industry Applications, IEEE Transactions on*, 45(4):1301 –1308, July 2009.

[7] W. Gruber, T. Nussbaumer, H. Grabner, and W. Amrhein. Wide air gap and large-scale bearingless segment motor with six stator elements. *Magnetics, IEEE Transactions on*, 46(6):2438 –2441, June 2010.

[8] J. Amemiya, A. Chiba, D.G. Dorrell, and T. Fukao. Basic characteristics of a consequent-pole-type bearingless motor. *Magnetics, IEEE Transactions on*, 41(1):82 – 89, Jan. 2005.

[9] S. Silber, W. Amrhein, P. Bösch, R. Schöb, and N. Barletta. Design aspects of bearingless slice motors. *Mechatronics, IEEE/ASME Transactions on*, 10(6):611 – 617, Dec. 2005.

[10] T. Reichert, J.W. Kolar, and T. Nussbaumer. Design study for exterior rotor bearingless permanent magnet machines. In *Energy Conversion Congress and Exposition (ECCE), 2011 IEEE*, pages 3377 –3382, Sept. 2011.

[11] T. Reichert, T. Nussbaumer, and J.W. Kolar. Bearingless 300-w pmsm for bioreactor mixing. *Industrial Electronics, IEEE Transactions on*, 59(3):1376 –1388, March 2012.

[12] B. Warberger, R. Kaelin, T. Nussbaumer, and J.W. Kolar. 50-nm 2500-w bearingless motor for high-purity pharmaceutical mixing. *Industrial Electronics, IEEE Transactions on*, 59(5):2236 –2247, May 2012.

[13] S. Silber and W. Amrhein. Force and torque model for bearingless pm motors. In *Proceedings International Power Electronics Conference (IPEC), Vol. 1, Tokyo*, April 2000.

[14] W. Gruber, W. Amrhein, S. Silber, H. Grabner, and M. Reisinger. Theoretical analysis of force and torque calculation in magnetic bearing systems with circular airgap. In *8th International Symposium on Magnetic Suspension Technology (ISMST8), 26. - 28. September 2006, Dresden, Deutschland*, 9 2005.

[15] S. Silber and W. Amrhein. Power optimal current control scheme for bearingless pm motors. In *7th International Symposium on Magnetic Bearings (ISMB), Zurich, Switzerland*, pages 401–406, Aug. 2000.

[16] H. Grabner, S. Silber, and W. Amrhein. Bearingless torque motor - modeling and control. In *Proc. 13th International Symposium on Magnetic Bearings*, 2012.

[17] H. Grabner. *Dynamik und Ansteuerkonzepte lagerloser Drehfeld-Scheibenläufermotoren in radialer Bauform*. Trauner Verlag, Linz, 2007.